

Ultraviolet images of the gravitationally lensed quadruple quasar Q2237+0305 with the *HST*¹ WFPC2

Michael Blanton, Edwin L. Turner
Princeton University Observatory, Princeton, NJ 08544
blanton, elt@astro.princeton.edu

and

Joachim Wambsganss
Astrophysikalisches Institut Potsdam, 14482 Potsdam, Germany
jwambsganss@aip.de

ABSTRACT

We present and analyze observations of the quadruple lensed quasar Q2237+0305, obtained with the *HST* WFPC2 camera in the F336W and F300W filters. Twenty-five exposures were performed within 15 hours real time on 3 November 1995. On a timescale of 3–4 hours, we observe no variation in component A of greater than 0.02 mag. The other components remain constant over a period of 10 hours to within about 0.05 mag. In the final 5 hours there is some evidence (not conclusive) for variation of component D by about 0.1 mag. The exposures indicate that component A is brighter than component B by about 0.3 mag. Components C and D are fainter than component A by about 1.3 and 1.4 mag, respectively. Our results place an upper limit on any fifth (central) component of 6.5 mag fainter than component A.

We determine the astrometric properties of the lens system, using only the exposures of the higher resolution Planetary Camera chip. We measure the relative distances of the four components with high accuracy. Our values are systematically larger than those of other investigators (by 0.1% to 2.0%). We discuss the reasons why we believe our results are reliable.

The F336W filter had been chosen for the observations because it corresponds to the redshifted Ly- α line of the quasar. This filter might have allowed us to see extended Ly- α emission from the Broad-Line Region (BLR) of the quasar as Ly- α arcs, and hence to determine the physical size of the BLR. However, the

¹Based on observations with the NASA/ESA *Hubble Space Telescope*, obtained at the Space Telescope Science Institute, which is operated by AURA under NASA contract NAS 5-26555.

quasar components in this filter are consistent with a point source. We conclude that there cannot be any Ly- α feature in the image plane brighter than about 23.5 mag in F336W and further from the quasar core than 100 mas. According to a lensing model by Rix, Scheider & Bahcall (1992), this would preclude any such features in the source plane further than 20 mas ($\sim 100h^{-1}$ pc, assuming $q_0 = 0.5$) from the quasar core and brighter than 25 mag before magnification.

Subject headings: gravitational lensing, quasars: individual: Q2237+0305

1. Introduction

The quasar Q2237+0305 at redshift $z = 1.695$ is gravitationally lensed by a nearby galaxy at $z = 0.039$ (Huchra *et al.* 1985). The galaxy core lies nearly perfectly along the line of sight. Such a configuration results in a symmetric, cross-like arrangement of the four quasar component images, with relative separations in this case between 1.2 and 1.8 arcsec.

Several facts make this lens system useful. First, the closeness of the lensing spiral galaxy allows us to study it in great detail. Second, the large leverage between lens plane and source plane that results from this proximity reduces the time scale for microlensing. Third, the symmetric arrangement of the four components leads to a small relative time delay (of order a day or shorter, *cf.* Wambsganss & Paczyński 1994). This last fact helps to distinguish intrinsic fluctuations of the quasar from microlensing-induced changes: the former have to show up in all four components almost simultaneously, whereas the latter are completely independent of each other, and occur on a timescale of months. Finally, the fact that the four quasar components are bright, well separated, and of comparable optical brightness makes Q2237+0305 an easy target for various photometric, spectroscopic and astrometric studies.

Recently, Q2237+0305 was detected at radio wavelengths with the VLA at 3.6cm and 20cm (Falco *et al.* 1996). The relative positions of the components measured in radio agree well with the optical positions. Furthermore, the relative flux ratios of the components in each wavelength regime are similar, with the exception that component D is brighter in the radio, compared with the optical light. Thus, the relative brightnesses in radio agree much better with the ratios predicted by various models (Rix, Schneider & Bahcall 1992), than do those in the optical; the slight discrepancy in the optical is possibly caused by a

demagnification due to microlensing (*cf.* Wambsganss, Paczyński & Schneider 1990; Witt & Mao 1994), or by dust in the lensing galaxy.

The system Q2237+0305 was the first in which microlensing was detected (Irwin *et al.* 1989; Corrigan *et al.* 1991). There are various photometric monitoring programs underway; these continue to show fluctuations in the component intensities which can be attributed to microlensing. Recent results of some of these campaigns were published by Lewis, Irwin & Hewett (1995), and Ostensen *et al.* (1996).

Here we present new data obtained with the WFPC2 camera aboard the Hubble Space Telescope. The motivation and the technical details of the observations are explained in Section 2. In Section 3 we present the results of these observations, including the photometry and the astrometry of the four components. We discuss our results and their implications in the final Section 4.

2. Motivation and Observations

The primary goal of the proposed observations was to use the Q2237+0305 lens system as a “Zwicky telescope,” *i.e.* to take advantage of the lensing magnification which nature provides in this case to image the background QSO’s structure with unprecedented and otherwise unavailable resolution.

We chose Q2237+0305 in part because Yee & De Robertis (1991) had claimed to see Ly- α emission distinct from the quasar components, possibly resulting from an intense star-forming region associated with the quasar. In addition, the quasar’s distance redshifts the Ly- α line to 3270Å, which is available to HST but is not so red that the light of the lensing galaxy swamps the quasar image. High surface brightness, spatially extended structure in the quasar image will most likely appear in Ly- α . Such structure could result from the broad line region (BLR), from a larger and more quiescent quasar HII region, or possibly even from intense star formation regions in the host galaxy. Also, if we were so fortunate as to resolve the continuum emitting region in some way, it is also expected to be relatively bright in the UV. Meanwhile, the light of the relatively red bulge component of the lensing galaxy, through which we see the quasar components, provides little UV background to swamp low surface brightness parts of the source image.

We proposed obtaining deep WFPC2 images in the F336W and F300W bands. Both bands are near the Ly- α line, but Ly- α would appear brighter in F336W than F300W. This difference allows us to distinguish between continuum and Ly- α emission.

We hoped, in the most optimistic scenario, that this project could yield the first well-resolved UV image of a classical high redshift QSO and thus provide a fundamentally important datum in our attempts to understand quasars. A Ly- α ring image, similar to the radio “Einstein rings”, was an extreme but real possibility. Finally, even if no resolved images were detected, the data would provide useful upper bounds on sizes and surface brightnesses of structures near the core of this QSO and so are still of considerable interest.

On 3 November 1995, we obtained a total of twenty-five exposures using the WFPC2 camera aboard the Hubble Space Telescope. Ten of these images were exposed on one of the Wide Field chips; of these images, four were taken using the F300W filter and six were taken using the F336W filter. The Wide Field images were exposed for approximately 1200 sec each. The remaining fifteen images were exposed on the Planetary Camera chip; of these images, six were taken using the F300W filter and nine were taken using the F336W filter. The Planetary Camera images were exposed for approximately 800 sec each. Thus, we had four combinations of chip and filter. In addition, within each of these combinations, the images were dithered by approximately half-integer numbers of pixels (*e.g.* $2\frac{1}{2}$ or $5\frac{1}{2}$). This dithering procedure allowed us to recover resolution higher than that of the chips’ pixels. See Table 1 for details on all of these exposures.

The PC chip scale is 45.53 ± 0.02 mas/pixel, and the scale of the WF3 chip is 99.56 ± 0.04 mas/pixel (Holtzmann *et al.* 1995). Thus, the PC achieves finer resolution while the WF3 yields greater signal-to-noise. We would expect the WF3 chip to detect large and diffuse signals more readily than the PC chip, and the PC chip to better perceive features close to the quasar core. Additionally, the PC chip is more suited to astrometry than the WF3 chip. Because of contamination difficulties, the PC chip is also preferable for photometry.

For the purpose of some of the work described here, it was convenient to combine the various images. This combination required using the *IRAF*² routine `crrej` to remove cosmic rays, and the *IRAF* routine `drizzle` to account for the dithering of the images (Fruchter & Hook 1997). Thus, we obtained four final images: two filters (F300W and F336W) times two chips (PC and WF3). These four images appear in Figure 1.

Finally, we note that the field around Q2237+0305 is extremely empty in our UV images. Only two field stars of significant brightness were detected in our exposures, both of them on exposures 11–25 of Table 1, when the quasar appeared on the PC chip. One was

²*IRAF* is distributed by the National Optical Astronomy Observatories, which are operated by the Association of Universities for Research in Astronomy, Inc., under cooperative agreement with the National Science Foundation.

~ 17 mag and appeared on WF2; the other was ~ 19 mag and appeared on WF3. This dearth of field stars, and their absence on the PC chip, posed difficulties in the photometric and astrometric calibration.

3. Results

As well as addressing the issues related to the physics of quasars outlined in Section 2, these exposures provide excellent astrometric and good photometric information. Thus, before discussing the possibility of resolving a Ly- α emitting region in the lensed quasar, we describe our photometric and astrometric results. As we outline below, we obtained most of these results from the uncombined images. In order to obtain the position of the galaxy core, however, it was necessary to use the combined images. Finally, we examine the possibility of a resolvable BLR or continuum-emitting region, using the combined images to obtain maximum signal-to-noise.

3.1. Photometry

We measure the relative brightness of the four quasar components A, B, C, D (identified in Figure 1) in each of the twenty-five exposures, using the *IRAF* procedure `qphot`. The zeropoint magnitudes for the STMAG system used here (the constant flux system used by Space Telescope) were derived from the `PHOTFLAM` values associated with each filter and chip. The errors in the zeropoints are about 0.02 mag (Holtzmann *et al.* 1995). The other major source of error is contamination, which accumulates on the WFPC2 after each monthly decontamination and degrades the throughput of the instrument. The effect of contamination is more severe for filters of shorter wavelength, and varies between the chips. For F300W and F336W, it is about 0.01 – 0.05 mag. Following Whitmore, Heyer & Baggett (1996), we used the `synphot` package and a synthetic quasar spectrum with $z = 1.695$ to estimate the effect of contamination in our case. Our results yield about 0.01–0.02 mag contamination in the PC chip, and 0.04–0.06 mag contamination in the WF3 chip. Because the contamination corrections are rather uncertain, we use only the PC chip to obtain the overall photometry. We average our results for each filter in the PC chip and list them in Table 2. The errors listed there are simply the 1σ variance found in the determination of the mean, added in quadrature with the errors expected in the zeropoint and in the contamination correction (~ 0.01 mag in F336W, ~ 0.02 mag in F300W).

In Figures 2a and 2b, we examine the time dependence of the component brightnesses

by plotting the photometry for each image of Table 1. Most of the exposures of the A component on WF3 have saturated pixels and are therefore not included in the plot. Other exposures are not included because cosmic rays interfere with the determination of their photometry.

It is useful to examine two time scales. First, because of the contamination and zeropoint uncertainties, we examine each chip/filter combination separately. This examination probes a timescale of only 3–4 hours, but allows us to assume that zeropoint and contamination problems are uniform for a single chip/filter combination. Accordingly, the error bars on the data points in Figures 2a and 2b do not include the zeropoint and contamination errors, but only the statistical photometric errors convolved with 0.01 mag pixel-centering errors. To test for variation, we compare the measured 1σ (σ_{obs}) dispersion about the mean (dotted lines Figures 2a and 2b) with the estimated 1σ (σ_{est}) errors on the data points. If the ratio $\sigma_{\text{obs}}/\sigma_{\text{est}}$ of these two quantities were large, we could claim possible variation. For comparison, for our 17 mag field star on WF2 $\sigma_{\text{obs}}/\sigma_{\text{est}} \sim 1.5$. For the quasar, in the PC chip, $\sigma_{\text{obs}}/\sigma_{\text{est}}$ exceeds 1 only for the B component in the F336W filter; this exception is due to a single anomalously bright image of B which we do not believe is intrinsic variation. In the WF3 chip, the situation is more difficult, especially in the F336W filter, where for the B, C, and D components $\sigma_{\text{obs}}/\sigma_{\text{est}} \sim 2$. Excepting these final images, we state that over the first 10 hours component A remains constant to within 0.02 mag and the other components remain constant to within 0.05 mag.

To examine the situation in the last 5 hours more thoroughly, we plot D–B and C–B magnitude differences in F336W versus time in Figure 3. The error bars and dotted lines have the same meanings as in Figure 2. We notice that while C and B remain at constant relative brightness throughout the run, and between the PC chip to the WF3 chip, D brightens relative to B and C in the final three images. Namely D–B changes by about 0.1 mag over the course of about 1.5 hrs. It is possible that this change is due to either intrinsic variability of the quasar or microlensing. We note that it is more likely that D brightens than that B and C dim. First, an explanation due to microlensing would clearly require two unlikely coincidences: that images B and C would start to vary at the same time and by the same amount; second, since the estimates of the time delay between B and C from lens models are typically ~ 10 hours (Rix *et al.* 1992), intrinsic variation of the quasar source would not cause them to vary together either. It is worth noting that the variations of B, C, and D, taken individually, are not excessive in these last three images ($\sigma_{\text{obs}}/\sigma_{\text{est}} \sim 2$ compared to 1.5 for a field star). Therefore, we cannot exclude that the large change in D–B is simply a coincidence between the errors in components B, C, and D; that is, that B and C just happen to appear somewhat dim in these images and that D just happens to appear to brighten.

To investigate the second interesting time scale, we look at the difference between the photometry on the PC chip and on the WF3 chip in each filter; this examination extends the timescale to ~ 8 hours for F300W and ~ 15 hours for F336W, but increases our errors because we have to account for the zeropoint and contamination difficulties. In fact, a glance at Figures 2a and 2b show that there must indeed be large contamination correction or zeropoint errors, as there are shifts in the apparent magnitudes of up to 0.1 mag halfway through the run, when we changed to the WF3 chip. Thus, although the PC and WF3 magnitudes are separated by 3σ even when we account for contamination correction and zeropoint errors, we do not regard these differences as intrinsic. (Note that any zeropoint and contamination errors do not affect our above conclusions regarding B–D).

Photometry in the F336W filter was performed by Rix *et al.* (1992). Their results agreed with ours for components A and D, but they found components B and C to be significantly brighter than we did (about 0.4 magnitudes each). Note that the color differences between components (presumably due to reddening by the galaxy core of the C and D components) preclude a meaningful comparison of our relative brightnesses to those observed in bands other than F336W or F300W.

3.2. Astrometry

Since the PC chip is better suited to astrometry than the WF3 chip, we measure the quasar and galaxy positions using only the PC chip. For each of the fifteen exposures on this chip, we determine the position of each quasar component (*A*, *B*, *C*, and *D*) using the *IRAF* procedures `imcentroid` and `metric`. Because the foreground galaxy has such a weak signal in our bands, we neglect the effect of any gradient in the galaxy light distribution on our calculated positions.

Because there are small rotations of the camera from exposure to exposure, we want to define the quasar geometry in a way which does not depend on the (slightly uncertain) orientation of the camera. Thus, we pick five quasar component pairs (*AB*, *CB*, *DB*, *AC*, and *DC*) and for each exposure measure the distances between the members of each pair. Thus, after measuring the positions of *A*, *B*, and *C* in an exposure, we can calculate the distances *AB*, *BC*, and *AC*. Even if the camera orientation changes from image to image, these distances should remain constant, as they are invariant under rotation. Indeed, they are quite constant, and we are able to average their values over all the exposures. These distances are listed in Table 3. Note that the standard deviations are all approximately 1.5 mas. When we perform the same procedure on the WF3 images, they yield results which are consistent with those of the PC chip, but with standard deviations of order 10 mas.

Since the galaxy is quite dim in the F300W and F336W filters, it is necessary to measure the position of its core using coadded images. We coadd the F300W exposures and F336W exposures separately, measure the distance of the galaxy core from components B and D in both coadded images, and then average the results to obtain the distances BG and DG listed in Table 3. Such a measurement is not as accurate as the distance determinations between the (point-like) quasar components, since the images undergo at least one shifting operation in the process of being coadded, in addition to being subjected to cosmic-ray rejection algorithms. Furthermore, the galaxy core is not point-like, but rather extended. Thus there could be systematic errors in the BG and DG distances which are larger than the statistical errors listed.

We use these distances to compare our results to those of other investigators. Essentially, the distances provide a more robust comparison of results than coordinates do because of the rotation problem described above; using distances instead of coordinates eliminates the need to worry about whether somebody else’s coordinate system is exactly lined up with ours. In rows two through six of Table 3, we have listed the results of a number of other investigators.

Immediately it is clear that our results differ systematically from most of the previous results. In particular, our distances are between 0.1 – 2.0 % larger than those of all other investigators. Only for the BG distance is our result smaller. This observation raises the possibility that we have determined our absolute scale inaccurately. Nevertheless, because the WFPC2 is not limited by atmospheric seeing, because it is a high quality post-repair *HST* observation, and because it is in a band in which the galaxy is faint, we are still confident of our results. The deflection angles and hence image separations in a simple gravitational lens system are proportional to the lens mass enclosed by the images; thus, our result implies an increase of 0.2 – 4.0% for this quantity, assuming a singular isothermal sphere model. This factor would be negligibly small compared to uncertainties in almost any other system, but detailed modeling of Q2237+0305 yields a mass for the inner region of the lensing galaxy which is thought to be accurate at such a level (Rix *et al.* 1992).

Here we discuss possible reasons for the systematic discrepancies between our astrometric results and those of others. Yee (1988), whose values are consistently about 1.5σ below ours, measured his astrometry in wavelengths ranging from 495 nm upwards. It is possible that the shape of the quasar region that dominates at these higher wavelengths is different than the shape of the region that dominates around 300 nm; such a shape difference could cause a slightly different image configuration. Probably a more important effect is that in the higher wavelengths, the foreground galaxy is bright, and the gradient of its light distribution can skew the determined positions of the quasar components. Of

course, he accounted for this effect using an iterative method which fit for the galaxy light distribution and the quasar component positions together. However, this procedure demands an accurate knowledge of the PSFs, and can be unreliable. The same comments apply to the results of Irwin (1989) and Racine (1991); furthermore, Racine (1991) determined his plate scale by scaling his results to those of Yee (1988), and therefore did not produce an independent result. Finally, Rix *et al.* (1992) and Crane *et al.* (1991) both suffer from the fact that the astrometry was performed with a pre-repair *HST* instrument. It is worth noting, however, that the Rix *et al.* (1992) results do agree with ours within their 1σ error bars, though their individual values are consistently smaller than ours.

Ideally, one would prefer to approach this question of scale by measuring the angular distance to a field star from the quasar components. Unfortunately, there are no stars on the PC chip in our exposures bright enough to yield reliable astrometry. There do exist two field stars that appear in the WF2 and WF3 chips during our PC exposures. However, even though the *IRAF metric* routine will yield astrometry for these relative to the quasar in the PC chip, such measurements would not yield unambiguous information about the scale of the PC chip, since the WF3 scale would also be included in the measurement. In addition, most of the other investigators either had to mask the relevant comparison stars because of their brightness (Racine 1991), did not have it in their field of view (Crane *et al.*, 1991), or had our problem, that the stellar image was on a different chip than the quasar (Rix *et al.* 1992). So measuring such an angular distance would not help to compare our results with other measurements.

Although for the purpose of comparing datasets it is preferable to measure distances, for modeling the system it is more useful to have the positions given in a particular coordinate system. Therefore, we also have listed in Table 2 the right ascension and declination displacements relative to component A, in units of arcsec. Note that the errors are the same as the errors in the distances of Table 3; that is, we do not include the errors incurred because of the uncertainty in determining the coordinate system.

3.3. Limits on the Size of the BLR of the quasar

The main purpose of these observations was to place limits on or, with luck, detect the size and brightness of the broad-line region (BLR) possibly associated with the quasar. The idea was that even if the unlensed BLR of the quasar were slightly smaller than the pixel size and its brightness below the detection limit, the BLR would be stretched and magnified due to the lensing magnification, so that one could possibly see arc-like structures. For this purpose it was best to use the combined images; however, one must temper any enthusiasm

for the resulting signal-to-noise and resolution gains by the awareness of possible spurious signals created by the combination process.

We employed two methods to examine possible tangential extension of the broad-line region. The first consisted of a mostly qualitative examination of quasar components and their colors; the second consisted of a quantitative examination of what sort of signal we could possibly detect around the quasars.

Upon examining the images visually, it seems clear that there is no measurable tangential extension. This absence is evident in Figure 4, which depicts a sum of all the components for the F336W exposure in the PC chip. In an attempt to detect a tangentially extended component in the image, we rotated our image of each component into a coordinate system such that the center of the galaxy was along the horizontal to the left, and the clockwise direction tangent to the galaxy was vertically down. Then we combined all of the images, scaling each to the same magnitude before combination. Presumably, such a depiction would enhance any tangential extension, which would appear vertically in Figure 4. The image here is nearly circularly symmetric, but the contours are $\sim 5\%$ longer in the vertical direction than in the horizontal direction. Similar images created for the other filter/chip combinations showed approximately the same result. We know that there is asymmetry in the PSF; however, since we rotate the image of each component before summing, we expect that this asymmetry is suppressed to some degree. To evaluate the completeness of this suppression, we perform the same rotation and summation, using as the base image a field star of about 17 mag on the WF2 chip (thus, instead of starting from four separate images we start each rotation from the same image). In the F336W filter, the resulting asymmetry amounted to $\sim 5\%$ excess in the vertical direction; in the F300W filter, the asymmetry was 2–3%. We also performed the rotation and summation on synthetic PSFs produced by the program `tinytim` (Krist 1992). The contours determined for these combined images are also long in the vertical direction, by $\sim 2\text{--}4\%$. Therefore, we conclude that the slight ellipticity observed in Figure 4 cannot be considered a reliable signature of structure.

In addition to searching in general for tangential extension, we can search specifically for features due to Ly- α emission. Since F336W would transmit the red-shifted Ly- α emission approximately three to four times more efficiently than would the F300W filter, we can difference the two filters in an attempt to pick out such features. Because the images are brighter in general in the F336W filter, we found it best to scale the images accordingly before differencing; this scaling was designed to make the cores of the components cancel, so one could pick out features surrounding the core. As the components differ somewhat in color (C and D being redder than A and B), we performed this scaling and subtraction

separately for each component.

Figure 5 depicts this subtraction for the images in both chips. Note that in the PC exposures, the A and B components reveal a slight positive feature downwards and leftwards of each, at an angle of forty-five degrees from the negative-x axis and at a distance from the core of approximately 0.1 arcsec. There are at least three explanations of this feature to explore. First, it could be an image of a real BLR associated with the quasar. Second, it could be a result of the dithering process. Finally, it could result from a difference in the diffraction patterns for the two filters. We favor this third explanation.

If the features were images of a Ly- α region associated with the quasar, the region would have about 10^{-3} of the integrated brightness of the quasar. This explanation of the features could be confirmed if we could determine whether the features existed around the C and D components, as well; since these components are expected to have the opposite parity of A and B, a feature due to lensing would appear on the opposite side in C and D than in A and B. That is, a lensed feature appearing on the lower left in the A component would appear on the upper right of the C component. Unfortunately, the noise around the C and D components is too severe to allow such a test.

However, there is another property we would expect if the feature were due to a Ly- α region near the quasar. We would guess that the features would be oriented differently with respect to their associated components. In particular, we would guess that each feature would lie in a direction nearly perpendicular to the line connecting its associated component and the galaxy. The direction towards the galaxy at A differs from that at B by thirty degrees, so we would expect the line connecting the component and the feature at A to differ from that at B by a similar amount. However, both of the observed features are forty-five degrees from the x-axis, which argues against their interpretation as a BLR.

Since the dithering occurs along the same direction (forty-five degrees from the x-axis), we suspected that perhaps a problem with accounting for the dither had caused the feature. Thus, we experimented with putting artificial errors in the dithering shift; that is, we purposely misaligned the images before recombining them. If the feature had been caused by an error in the dithering, we would expect the misalignments to affect the feature. Although we tried misalignments as drastic as half a pixel, they had no effect on the feature. Therefore, we conclude that the dithering process most likely did not cause the feature.

The remaining explanation is that the diffraction patterns for the two filters differ enough that their difference causes a visible residual. As there are no bright stars in our exposures on the PC chip with which to test this proposition, we resort to the synthetic PSFs provided by the program `tinytim`. We subtract synthetic PSFs in the F336W and

F330W filters (subsampling by a factor of two, as the image in Figure 5 is). Because the diffraction ring patterns are of slightly different sizes in the two filters, one obtains a pattern of rings in the differenced image. Examining the first positive ring from the center, we discovered that it was about the same distance from the center and about the same brightness as the features in the real images; interestingly, it had an asymmetry that caused it to be brighter on the lower left than elsewhere along the ring. We avoid taking this result too literally, but we do conclude that the differing diffraction patterns of the two filters could cause the feature we see.

Even so, we can use this feature to place an upper limit on the brightness of compact regions that could exist without our detecting them. For the A component, the accompanying feature has an integrated brightness about 6.9 magnitudes dimmer than the component; the corresponding figure for the B component is about 7.5 magnitudes. Thus we can state with confidence that there is no Ly- α feature further than 100 mas from the quasar core and brighter than about 23.5 magnitudes in the F336W band. Using the lensing model of Rix *et al.* (1992), this would preclude any features further than 20 mas ($\sim 100h^{-1}$ pc, assuming $q_0 = 0.5$) from the quasar core in the source plane and brighter than 25 mag before magnification.

We can place another quantitative limit on the size and brightness of a tangentially extended image surrounding the quasar components. To do so, consider one of the quasar components. Draw a circle centered on it. Evaluate the F336W surface brightness at each point around that circle. This evaluation yields brightness as a function of angle. If the coordinates are such that the galaxy is in the direction $\theta = 0$, and the quasar component were tangentially extended, the brightness function would have bumps at $\theta = +90$ and -90 degrees. Upon examination of such plots, we see no such bumps. To place a limit on the size of bump we could measure, we calculate the standard deviation σ of the surface brightness values around the circle about their mean. Then we require some signal-to-noise ratio (S/N) for a meaningful result, and our limit becomes $(S/N)\sigma$.

Figure 6 reveals the results of this procedure for the images in the PC chip and the F336W filter, which is most likely to reveal Ly- α structure. The horizontal axis is the radius in mas, and the vertical axis is the standard deviation in flux units. Depending on the assumed lensing model, we may divide the radius by the appropriate magnification for each component to obtain the limits appropriate for the source plane; thus, we can use the lensing magnification to “squeeze” the plot radially. For example, a limit of 3×10^{-17} erg cm $^{-2}$ s $^{-1}$ arcsec $^{-2}$ at 100 mas, given a magnification of 5, would become a limit of 3×10^{-17} erg cm $^{-2}$ s $^{-1}$ arcsec $^{-2}$ at 20 mas. However, we are obliged to multiply the vertical axis by our desired signal-to-noise ratio; thus we must slide the plot up (on a logarithmic axis). In

the example above, our limit of 3×10^{-17} erg cm⁻² s⁻¹ arcsec⁻² at 20 mas, given a required (S/N) of 5, would yield, a limit of 1.5×10^{-16} erg cm⁻² s⁻¹ arcsec⁻² at 20 mas. The results of such a squeezing and sliding appear in Figure 7 for the model 2a of Rix *et al.* (1992), with a signal-to-noise ratio of 5.

We compare our two methods by noting that the brightest pixels in the features associated with the A and B components have a surface brightness of about 3×10^{-17} erg cm⁻² s⁻¹ arcsec⁻² and are located about 100 mas from each component. This position is indicated as a cross in Figure 6. Thus, the feature is just at our calculated threshold. With the conservative requirement of a 5σ result, as in Figure 7, this feature would be well below the noise. In Figure 7, we have included the source plane position of the feature on every plot; for this purpose we used its position as determined by its appearance next to the B component. That this feature is somewhat submerged in our predicted noise encourages our belief that Figure 6 provides a reasonable upper limit for the brightness of other possible features.

Finally, we can compare our results with other observations of regions surrounding high-redshift quasars, in particular those of Bremer *et al.* (1992). These investigators found extended Ly- α emission around two $z = 3.6$ quasars, at fluxes of approximately 10^{-16} erg cm⁻² s⁻¹ and extensions of about 4 arcsec. From our results, any emission at this level over such a large scale can be excluded for quasar Q2237+0305.

3.4. Limits on a Fifth Image

A final consideration is the possibility of detecting a faint fifth component of the quasar. Predictions of the brightness of this component relative to A are uncertain by orders of magnitude; for example, the results of Schneider *et al.* (1988) indicate $\Delta m > 3.5$, Kent & Falco (1988) find $\Delta m \approx 7.5$, and Rix, Schneider & Bahcall (1992) find $\Delta m > 5$ for all their models. In this regard, it is worth noting that the galaxy core is 6.5 mag dimmer than component A, and is close to the threshold of detectability. Since there is not the slightest indication of a fifth component in the image, it must be at least 6.5 mag dimmer than component A, in our filters F336W and F300W. Our results do not appear to support the findings of Racine (1991), who detected a faint fifth component 4.5 mag dimmer than A in the R and I bands. However, a central fifth component could be brighter with respect to A in longer wavelength bands as a result of reddening due to dust. The fifth component would shine through the very center of the lensing galaxy, making any extinction estimates wildly uncertain.

4. Summary and Conclusions

In this paper, we have presented the results of Hubble Space Telescope exposures on the WFPC2 camera of quasar Q2237+0305; specifications of the images are in Table 1 and we display the image configuration in Figure 1. The F336W and F300W filters were chosen because the relatively red galaxy bulge through which we see the quasar components is faint in the UV, and because one of the filters is very close to the redshifted Ly- α line of the quasar (at about 3270Å), so that it is plausible that any spatially extended structures in the quasar environment would emit in this wavelength regime. We have determined:

1. The photometry for the four components in the F336W and F300W bands, which is listed in Table 2. The relative brightnesses of the components are known to vary with time due to microlensing. At the time of our observations, component A was the brightest, followed by component B which was fainter by 0.3 mag. Components C and D were fainter than component A by about 1.3 and 1.4 mag, respectively. On the timescale of 3–4 hours, we can state that we observe no variation in component A of greater than 0.02 mag. For the other components, over a period of 10 hours they remain constant to within about 0.05 mag. In the final five hours there is some evidence for variation of component D of about 0.1 mag.
2. The astrometry of the four components and the galaxy core, which is listed in Tables 3 and 4. The (1σ -) uncertainty of these astrometric measurements are about 1.5 mas. We found the system to be consistently larger (by between 0.1% and 2%) than previous studies have found. We discuss above why we think our values are reliable.
3. The existence of a feature near the A and B components which is bright in F336W, as shown in Figure 5 with a subtraction of F300W from F336W. We conclude that this signal is probably an artifact of the differing diffraction patterns of the two filters. However, we use the brightness of the feature to obtain an upper limit on the brightness of any real Ly- α regions, plotted as the crosses on Figures 6 and 7.
4. An estimate of the upper limits these images yield for the brightness of any extended image near the quasar, as a function of angular distance from the quasar in the source plane. These upper limits depend on the lensing model and the desired signal-to-noise. They are plotted in Figures 6 and 7.
5. An upper limit on the brightness of central fifth component in our band which is 6.5 mag fainter than component A.

5. Acknowledgements

We wish to thank Ray Lucas, Jean Surdej, and Brad Whitmore of the Space Telescope Science Institute for useful help and advice. In addition, we would like to thank the authors of the `drizzle` algorithm, Andy Fruchter of STScI and Richard Hook of ST-ECF. We acknowledge financial support from STScI grant GO-05937.01-94A.A01.

REFERENCES

- Bremer, M. N., A. C. Fabian, W. L. W. Sargent, C. C. Steidel, A. Boksenberg, R. M. Johnstone: 1992, *Mon. Not. R. Astro. Soc.* **258**, 23P.
- Corrigan, R. T., M. J. Irwin, J. Arnaud, G. G. Fahlman, J. M. Fletcher, *et al.*: 1991, *Astron. J.* **102**, 34.
- Crane, P., R. Albrecht, C. Barbieri, J. C. Blades, A. Boksenberg *et al.*: 1991, *Astrophys. J.* **369**, L59.
- Falco, E. E., J. Lehar, R. A. Perley, J. Wambsganss, M. V. Gorenstein: 1996, *Astron. J.*, **112**, 897.
- Fruchter, A. and Hook, R.: 1997, *PASP*, Submitted.
- Huchra, J., M. Gorenstein, S. Kent, I. Shapiro, G. Smith, *et al.*: 1985, *Astron. J.* **90**, 691.
- Holtzmann, J., *et al.*: 1995, *Publ. Ast. Soc. Pac.* **107**, 156.
- Irwin, M. J., P. C. Hewett, R. T. Corrigan, R. I. Jedrzejewski, R. L. Webster: 1989, *Astron. J.* **98**, 1989.
- Kent, S. M. and E. E. Falco: 1988, *Astron. J.* **96**, 1570.
- Krist, J. 1992, The Tiny Tim User's Manual (Baltimore: STScI)
- Lewis, G. F., M. J. Irwin, P. C. Hewett: 1995, *Astrophys. J.*, submitted August 1995.
- Ostensen, R., S. Refsdal, R. Stabell, J. Teuber, P. I. Emanuelsen, *et al.*: 1996, *Astron. Astrophys.* **309**, 59.
- Racine, R.: 1991, *Astron. J.* **102**, 454.
- Rix, H.-W., D. P. Schneider, J. N. Bahcall: 1992, *Astron. J.* **104**, 959.
- Schneider, D. D., E. L. Turner, J. E. Gunn, J. N. Hewitt, M. Schmidt, and C. R. Lawrence: 1988, *Astron. J.* **95**, 1619.
- Wambsganss, J., B. Paczyński: 1994, *Astron. J.* **108**, 1156.

Wambsganss, J., B. Paczyński, P. Schneider: 1990, *Astrophys. J.* **358**, L33.

Whitmore, B., I. Heyer, S. Baggett: 1996, STSci Instrument Science Report WFPC2 96-04.

Witt, H.J., and Mao, S.: 1994, *Astrophys. J.* **429**, 66.

Yee, H. K. C.: 1988, *Astron. J.* **95**, 1331.

Yee, H. K. C., M. M. De Robertis: 1991, *Astrophys. J.* **381**, 386.

Table 1. Log of observations taken 3 Nov. 1995.

Exposure Number	Camera	Filter	Exposure Time (s)	Dither Offset (mas)
1	WF3	F300W	1100	0
2	WF3	F300W	1100	0
3	WF3	F300W	1300	250
4	WF3	F300W	1300	250
5	WF3	F336W	1100	0
6	WF3	F336W	1200	0
7	WF3	F336W	1200	0
8	WF3	F336W	1100	250
9	WF3	F336W	1200	250
10	WF3	F336W	1200	250
11	PC	F336W	700	0
12	PC	F336W	700	0
13	PC	F336W	700	0
14	PC	F336W	800	0
15	PC	F336W	700	0
16	PC	F336W	700	250
17	PC	F336W	800	250
18	PC	F336W	800	250
19	PC	F336W	800	250
20	PC	F300W	700	0
21	PC	F300W	800	0
22	PC	F300W	700	0
23	PC	F300W	700	250
24	PC	F300W	800	250
25	PC	F300W	800	250

Table 2. Photometric results for each component of lensed quasar Q2237+0305, in F336W and F300W filters (averaged over all PC exposures, cf. Table 1), and positions, obtained from the PC images. Photometric quantities are in the STMAG system; errors listed are the 1σ dispersions of the individual results about the mean, added in quadrature with the errors associated with the zeropoint and with the contamination correction. Astrometric quantities are given in arcseconds along the directions of right ascension and declination. As explained in the text, the astrometric errors do not include possible systematic errors in determining the orientation of the coordinate system.

Component	F336W Magnitude	F300W Magnitude	Right Ascension (")	Declination (")
A	16.65 ± 0.02	16.85 ± 0.03	0.000 ± 0.0015	0.000 ± 0.0015
B	16.93 ± 0.04	17.10 ± 0.03	-0.671 ± 0.0015	1.697 ± 0.0015
C	17.95 ± 0.03	18.24 ± 0.04	0.634 ± 0.0015	1.210 ± 0.0015
D	18.10 ± 0.03	18.41 ± 0.03	-0.866 ± 0.0015	0.528 ± 0.0015
Galaxy Core	N/A	N/A	-0.081 ± 0.010	0.937 ± 0.010

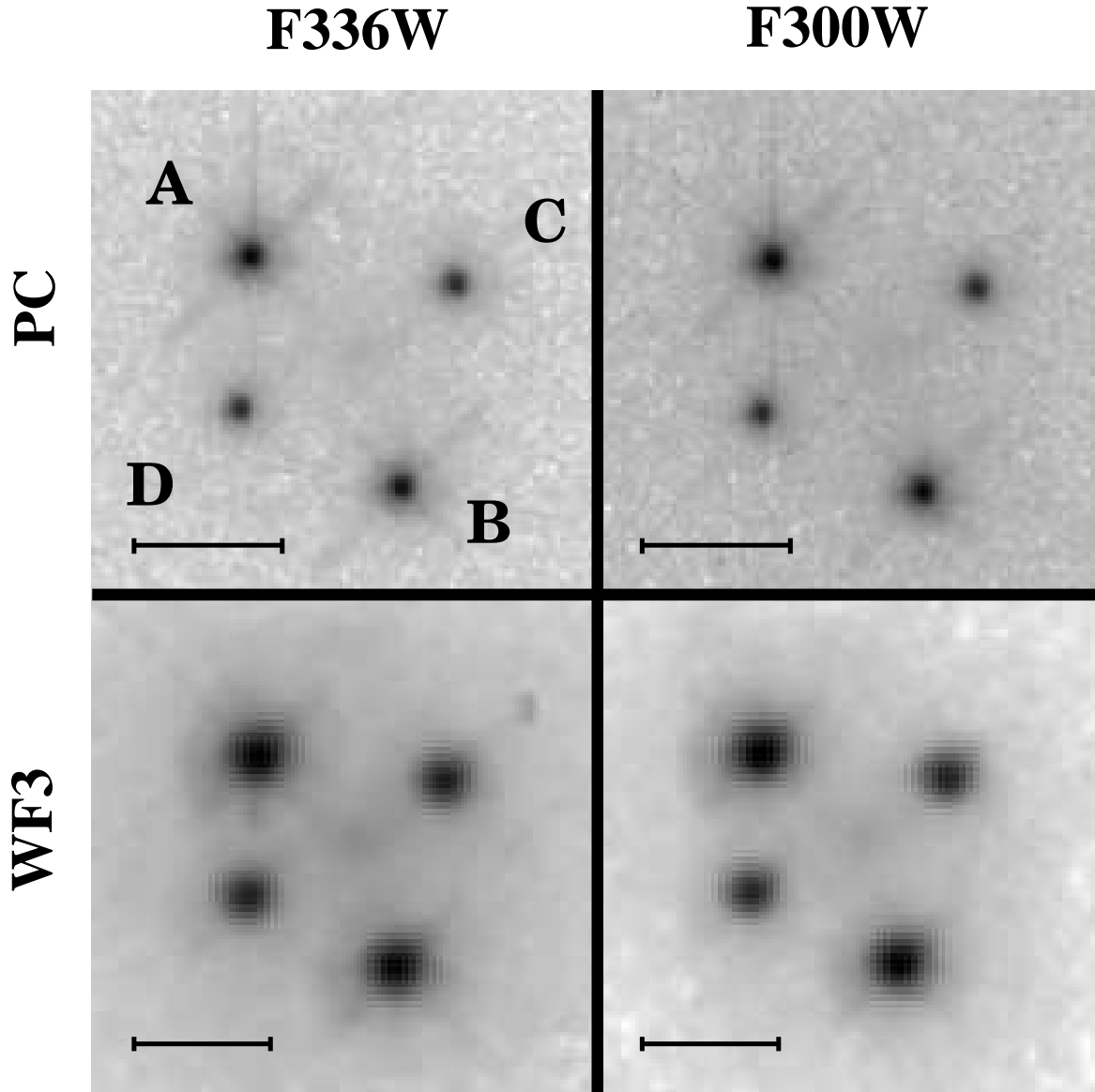


Fig. 1.— The full configuration of lensed quasar Q2237+0305. Components A, B, C, and D are labeled. The images in the top row were exposed on the PC chip; the scale indicates $1''$. The images in the bottom row were exposed on the WF3 chip; the scale indicates $1''$. The images in the left column used the F336W filter; those in the right column used the F300W filter. The feature near component C in the WF3 F336W exposure is a cosmic ray left over from the image processing.

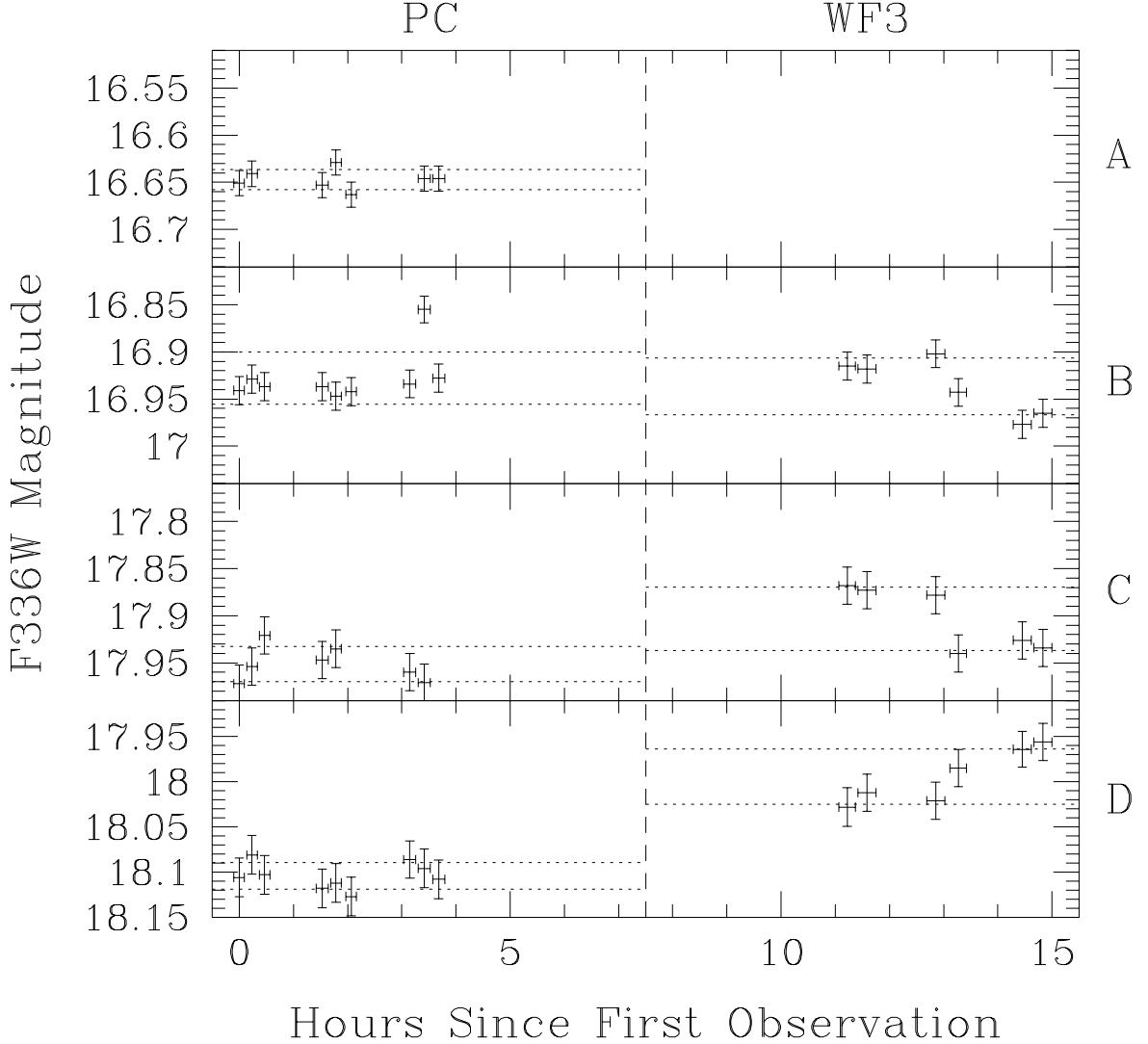


Fig. 2a.— The “lightcurve” of each component of lensed quasar Q2237+0305 in the F336W filter. The vertical error bars are 1σ limits determined only from the statistics of the photometry and the expected pixel-centering error of 0.01 mag; the horizontal error bars represent the duration of the exposure. Although these images are corrected for contamination, the error in that contamination correction is not included in the error bars. Note that the PC chip was used for the first half of the observations, while the WF3 chip was used for the second half. Dotted lines delimit the 1σ dispersion about the mean for the PC and WF3 exposures. Note that the A component was saturated for the final 8 exposures and therefore we did not plot those points; other points are missing because of contamination by cosmic rays.

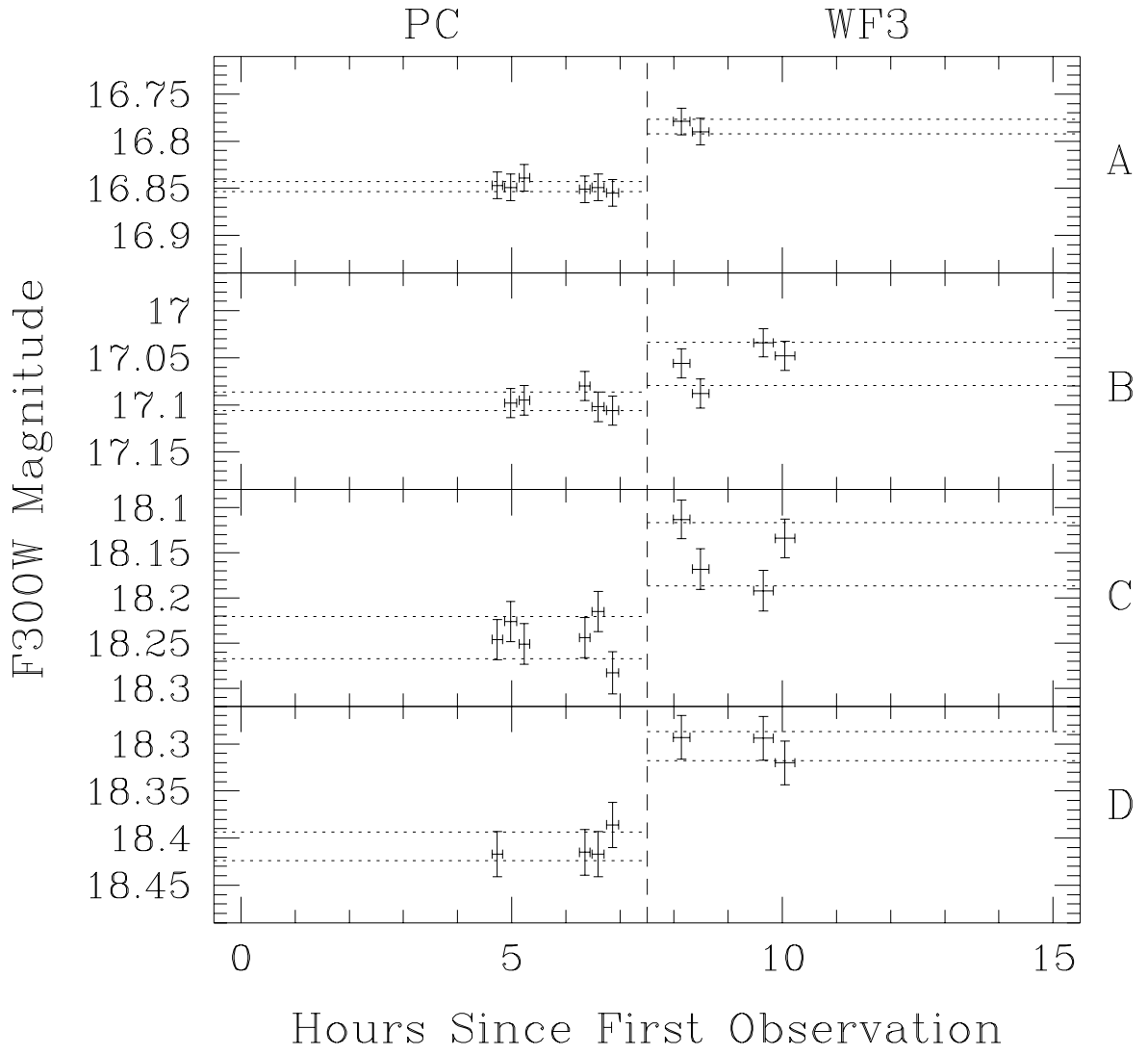


Fig. 2b.— Same as Figure 2a, for the F300W filter.

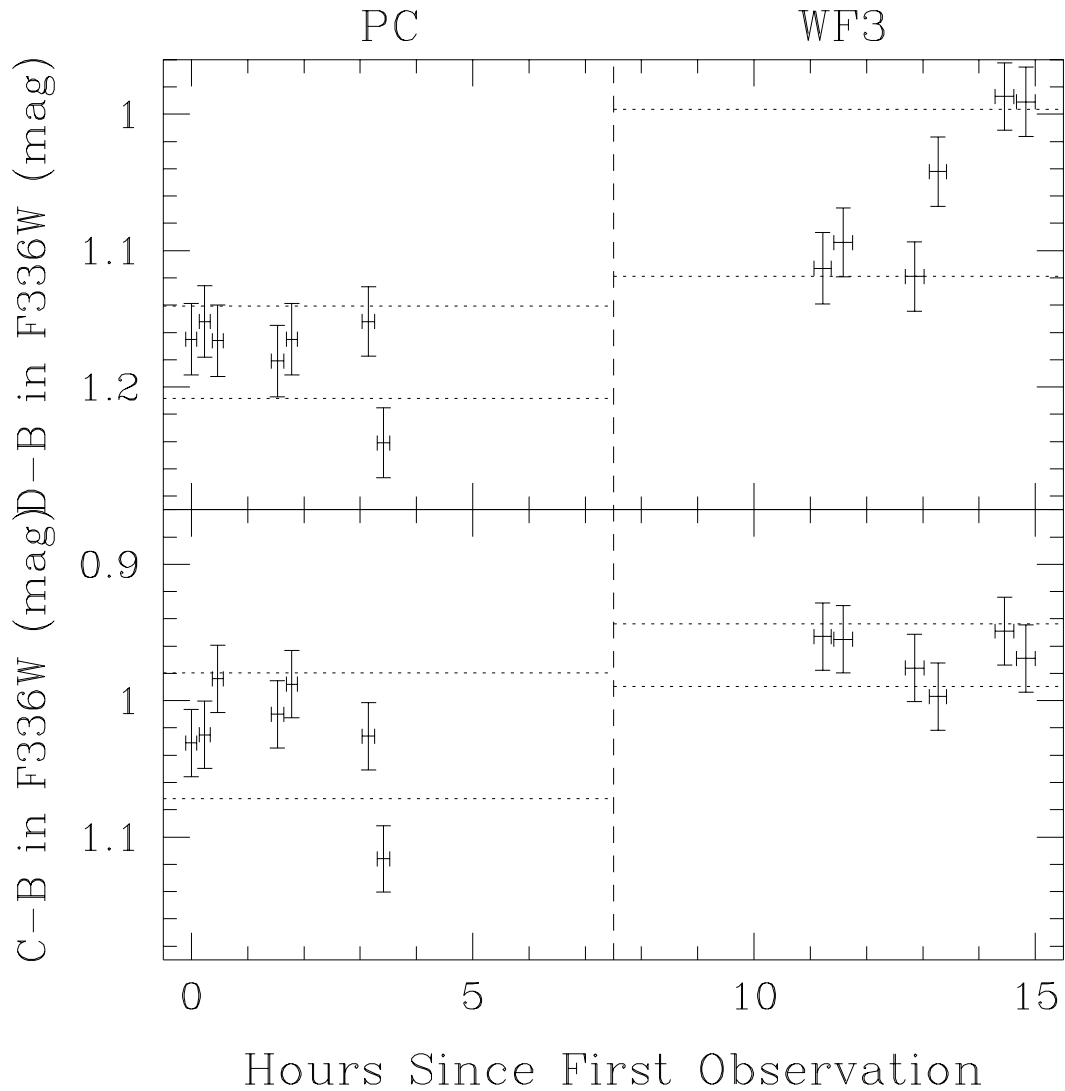


Fig. 3.— D–B and C–B magnitude differences for lensed quasar Q2237+0305 in the F336W filter. The vertical error bars are 1σ limits determined only from the statistics of the photometry and the expected pixel-centering error of 0.01 mag; the horizontal error bars represent the duration of the exposure. Dotted lines delimit the 1σ dispersion in the D–B and C–B values about their mean for the PC and WF3 exposures. Note the rise in D–B in the final three images.

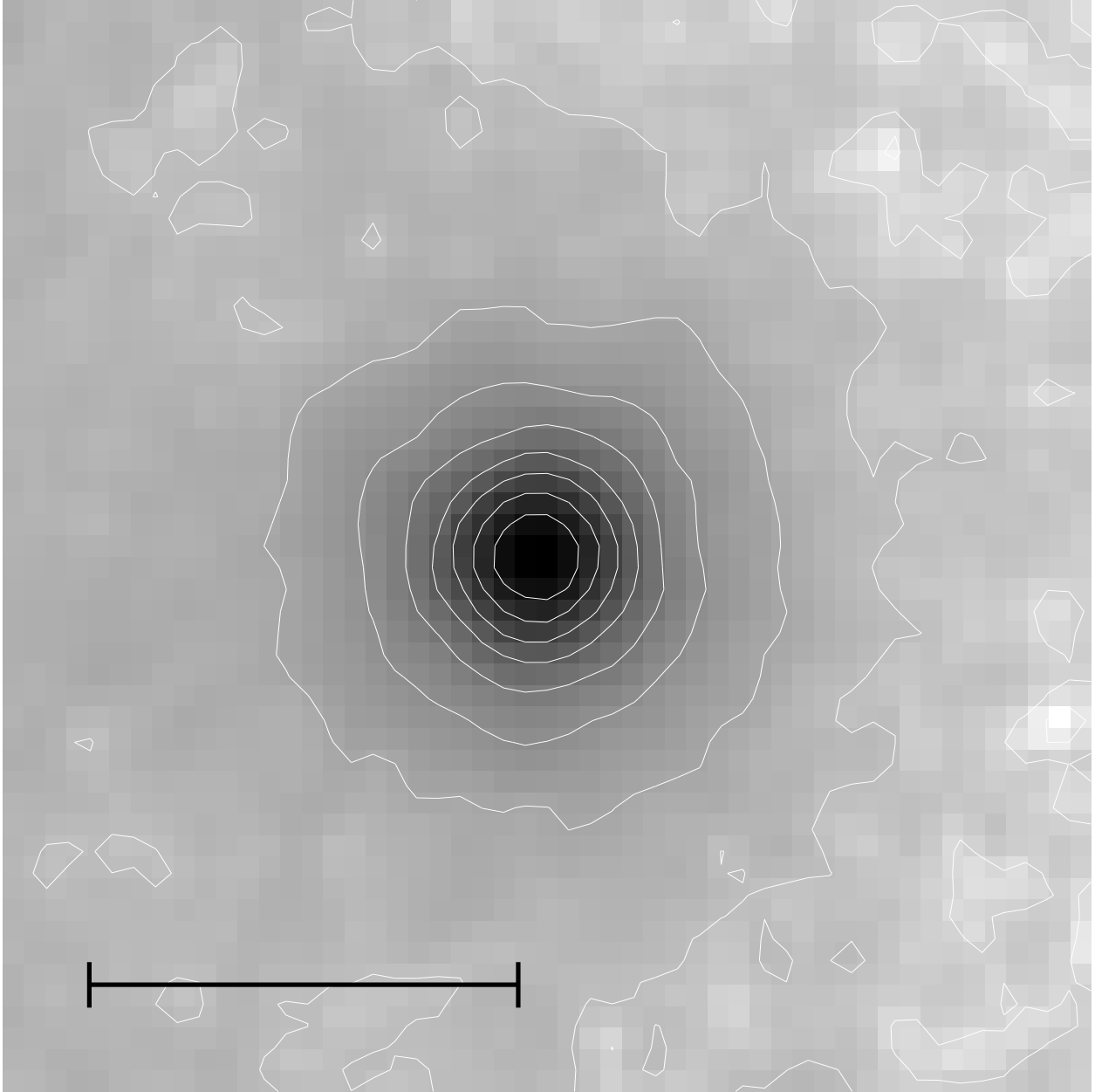


Fig. 4.— A sum of all the components of lensed quasar Q2237+0305 from the images taken in the PC chip with the F336W filter. We aligned the images of each component such that the direction to the galaxy is to the left of the page and the clockwise direction around the galaxy is down the page. The contours reveal about a 5% extension in the y-direction, which we believe to be consistent with no extension. The scale indicates $0.5''$.

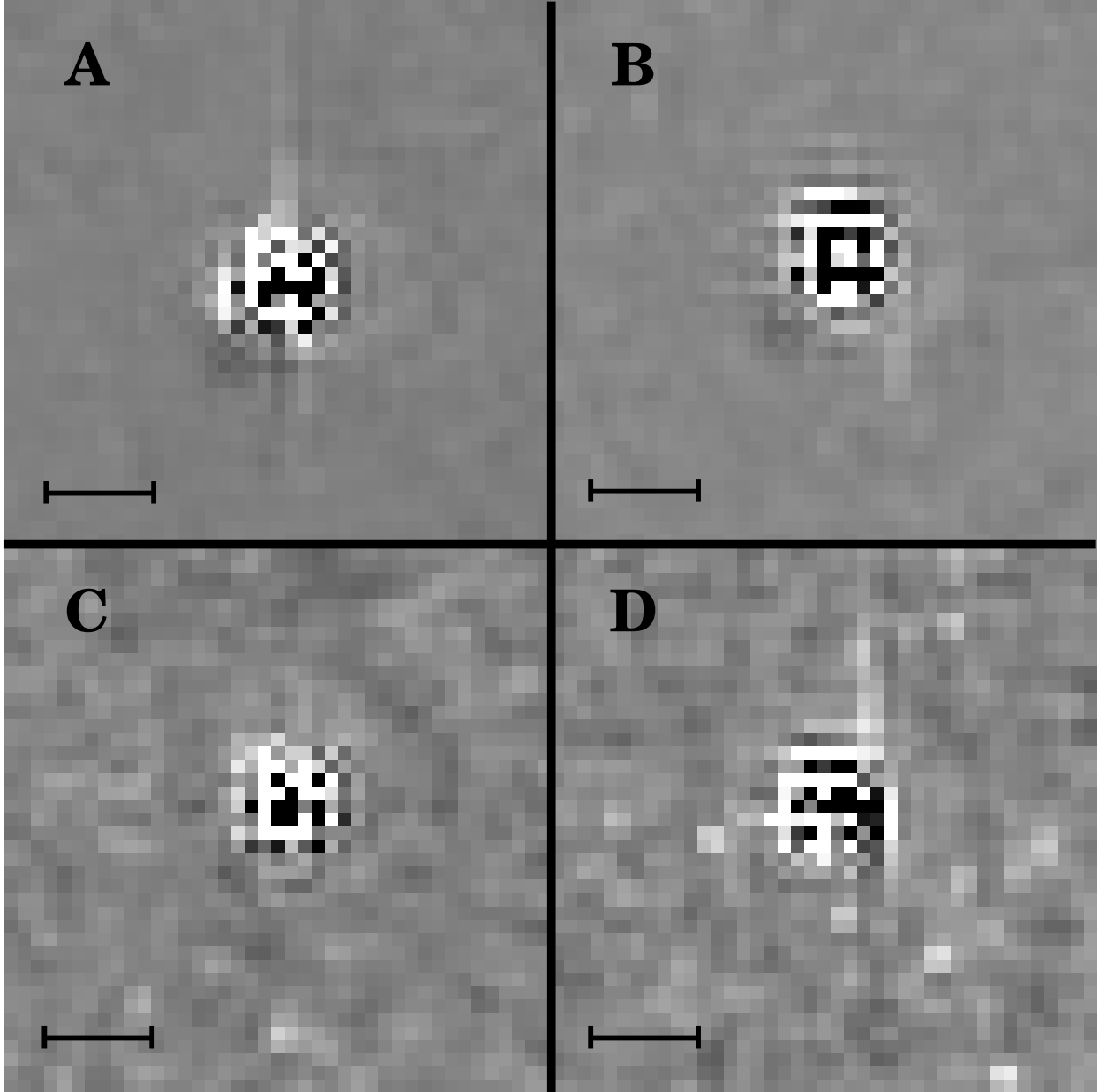


Fig. 5a.— The scaled differences between the F336W and F300W filter in the PC chip for each component of lensed quasar Q2237+0305. Darker colors indicate more intense F336W. Note the features on the lower left of components A and B. The scale indicates $0.2''$.

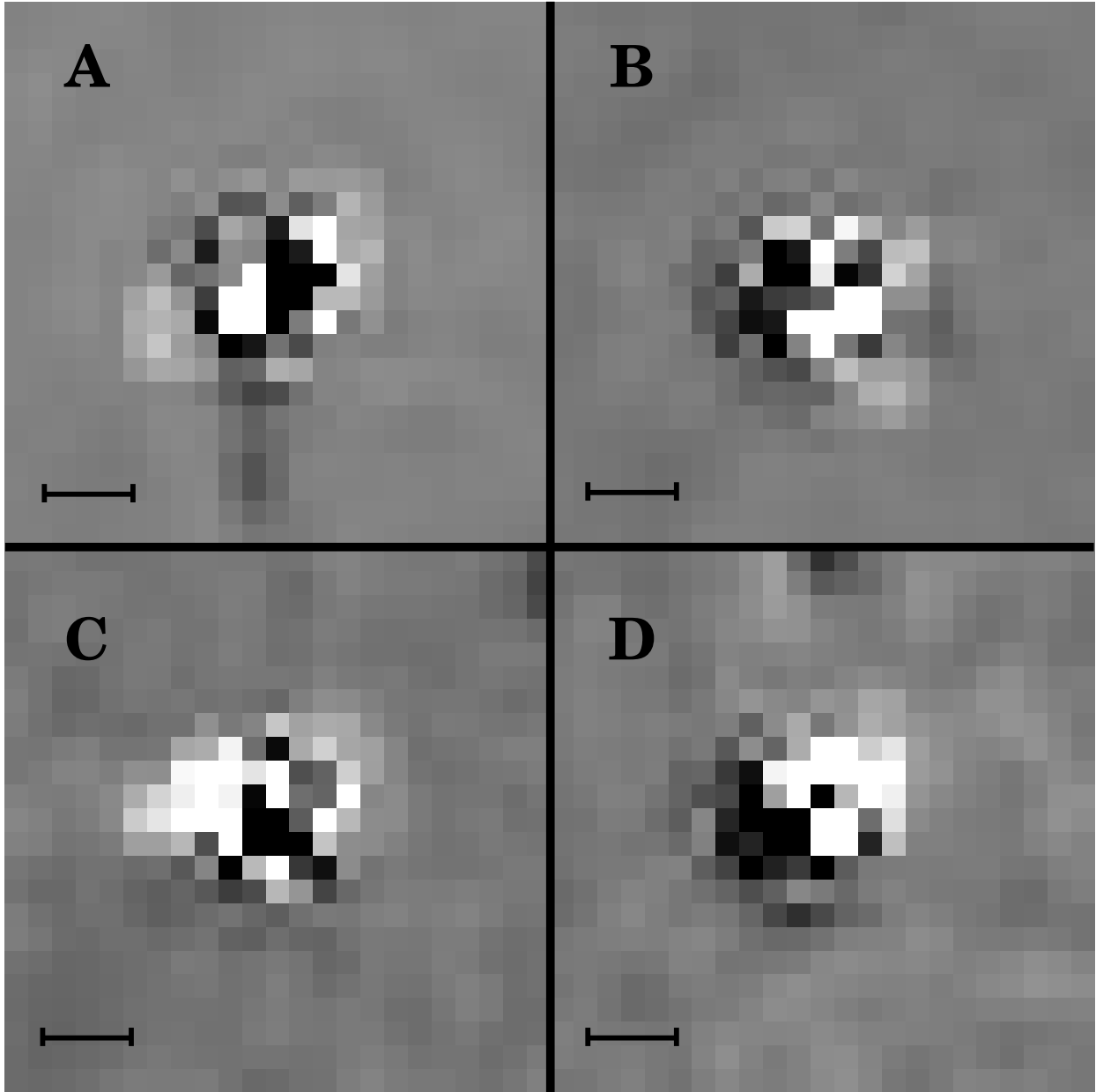


Fig. 5b.— Same as Figure 3a, but for the WF3 chip. The scale indicates $0.2''$.

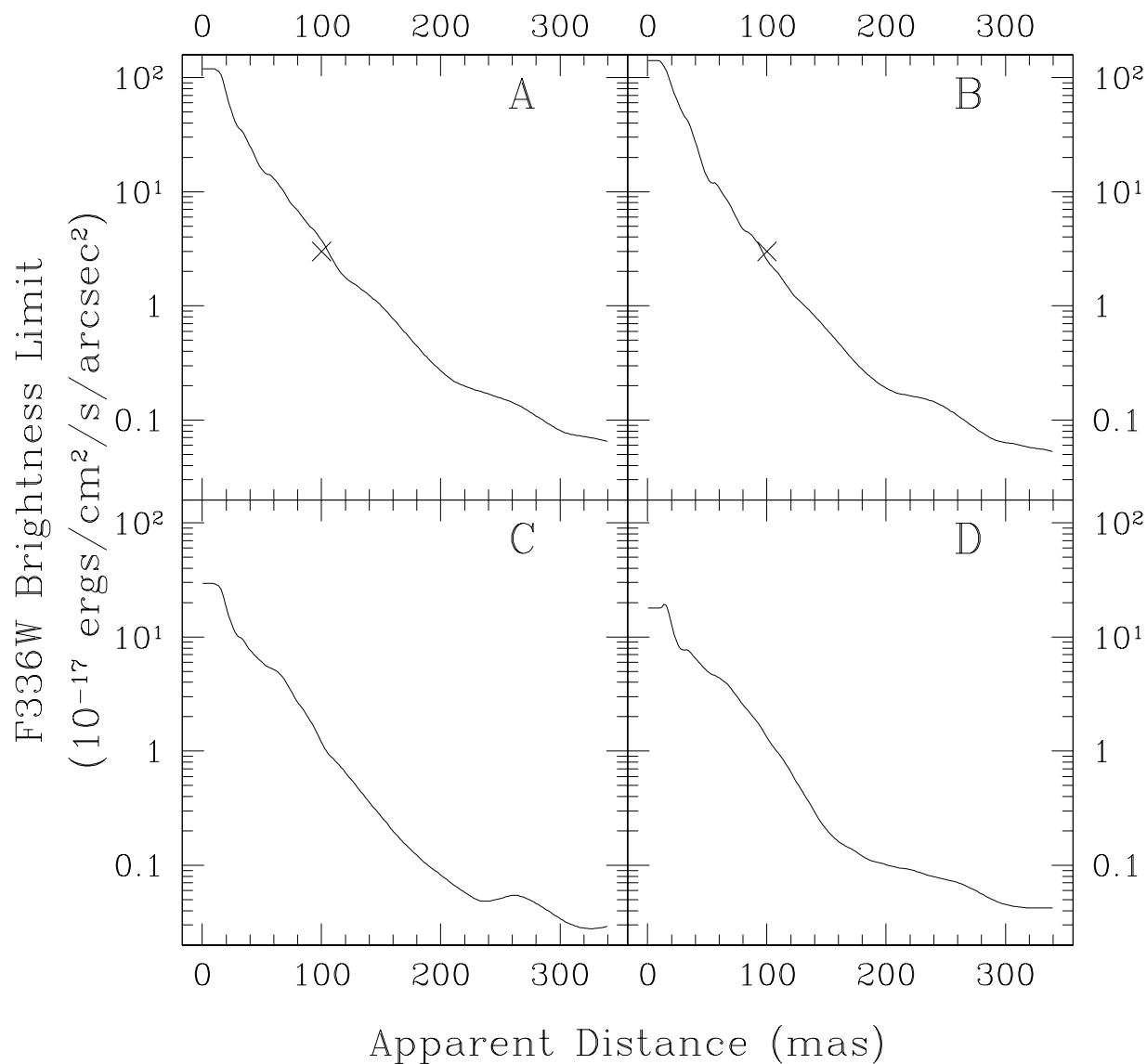


Fig. 6.— Limits on the brightness of a possible Lyman- α region, according to the PC chip in the F336W filter. Apparent distance is the angular distance measured on the sky. It equals the angular distance in the source plane multiplied by the magnification. The plotted curves correspond to 1σ limits. Crosses in the A and B plots indicate where the feature of Figure 3a lies.

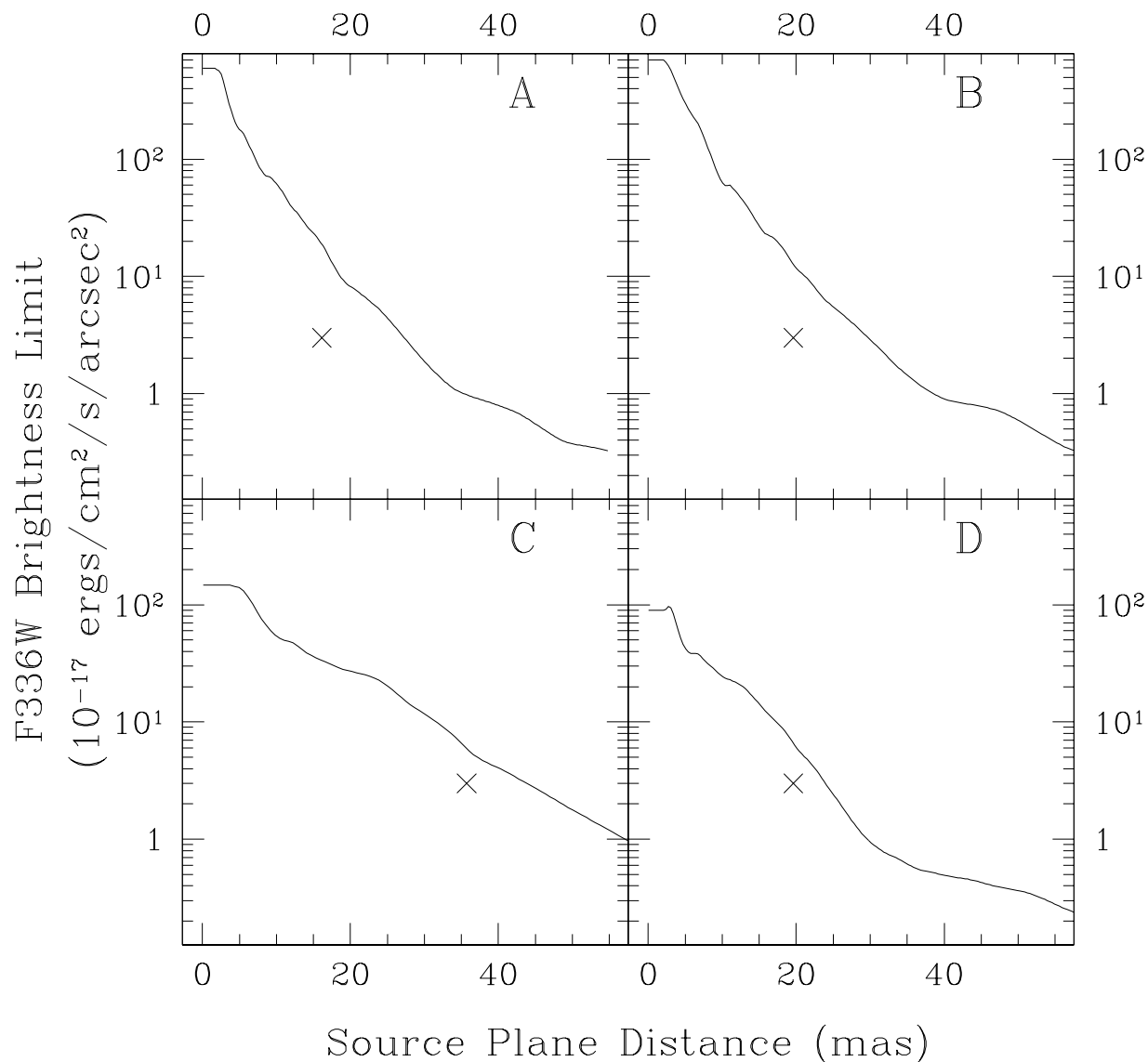


Fig. 7.— Limits on the brightness in the source plane of a possible Lyman- α region, according to the PC chip in the F336W filter. Magnifications are taken from the model of Rix (1992), and the curves correspond to a 5 σ result. Crosses indicate where the feature of Figure 3a would lie in the source plane; we determined its brightness and its position in the source plane by examining its incarnation next to the B component.

Table 3. Distances between components of lensed quasar Q2237+0305, as measured by various observers.

Investigator (instrument, year)	AB (")	CB (")	DB (")	AC (")	DC (")	BG (")	DG (")
This paper (WFPC2)	1.824 ± 0.0015	1.391 ± 0.0015	1.185 ± 0.0016	1.365 ± 0.0015	1.645 ± 0.0015	0.962 ± 0.007	0.884 ± 0.009
Rix et al. (WFPC1, 1992)	1.816 ± 0.015	1.389 ± 0.015	1.182 ± 0.015	1.353 ± 0.015	1.641 ± 0.015	0.970 ± 0.015	0.881 ± 0.015
Racine (CFHT, 1991)	1.811 ± 0.002	1.374 ± 0.002	1.166 ± 0.002	1.352 ± 0.002	1.617 ± 0.002	0.955 ± 0.002	0.880 ± 0.002
Crane et al. (FOC, 1991)	1.799 ± 0.005	1.381 ± 0.005	1.166 ± 0.005	1.356 ± 0.005	1.632 ± 0.005	0.934 ± 0.005	0.869 ± 0.005
Irwin et al. (CFHT, 1989)	1.822 ± 0.01	1.367 ± 0.01	1.164 ± 0.01	1.351 ± 0.01	1.606 ± 0.01	0.982 ± 0.01	0.877 ± 0.01
Yee (CFHT, 1988)	1.812 ± 0.01	1.386 ± 0.02	1.162 ± 0.02	1.351 ± 0.01	1.615 ± 0.02	0.953 ± 0.02	0.872 ± 0.02
Falco et al. (VLA, 1996)	1.776 ± 0.05	1.353 ± 0.06	1.148 ± 0.04	1.407 ± 0.08	1.628 ± 0.07	N/A	N/A